Charge carrier identification in tunneling spectroscopy of core-shell nanocrystals

T.H. Nguyen, Justin Habinshuti, Y. Justo, R. Gomes, G. Mahieu, S. Godey, J.P. Nys, S. Carrillo, Z. Hens, O. Robbe, et al.

Charge carrier identification in tunneling spectroscopy of core-shell nanocrystals

T. H. Nguyen,[1] J. Habinshuti,[1,2] Y. Justo,[3] R. Gomes,[3] G. Mahieu,[1] S. Godey,[1] J. P. Nys,[1] S. Carrillo,[1] Z. Hens,[3] O. Robbe,[4] S. Turrell,[2] and B. Grandidier[1,*]

[1]*Institut d'Electronique, de Microélectronique et de Nanotechnologie, IEMN-CNRS, Département ISEN, 41 bd Vauban, 59046 Lille Cedex, France*

[2]*Laboratoire de Spectrochimie Infrarouge et Raman, LASIR, Université des Sciences et Technologies de Lille, Bât C5, 59655 Villeneuve d'Ascq Cedex, France*

[3]*Physics and Chemistry of Nanostructures, Ghent University, Krijgslaan 281-S3, B-9000 Ghent, Belgium*

[4]*Laboratoire de Physique des Lasers, Atomes et Molécules (CNRS, UMR 8523), Bât P-5, Université de Lille 1, 59655 Villeneuve d'Ascq, France*

(Received 10 October 2011; revised manuscript received 7 November 2011; published 28 November 2011)

Semiconductor PbSe/CdSe core-shell nanocrystals (NCs) in a double barrier tunnel junction have been investigated by means of scanning tunneling spectroscopy at low temperature. From the analysis of the differential conductance peak position as a function of the potential distribution in both potential barriers, we demonstrate a unipolar transport regime for a large amount of NCs. The same charge carriers are injected on both sides of the zero-conductance gap, and the peaks observed at higher energy arise from the charging of the NCs. Similar results are obtained for CdSe/CdS dot-in-rod NCs, indicating that the addition of a shell favors transitions between different charge states rather than single particle excited states. Further characterization of the PbSe/CdSe core-shell NCs by x-ray photoemission spectroscopy reveals that the variations in the transport properties from NC to NC are explained by the occurrence of unprotected PbSe facets that have different orientations in the junction.

DOI: 10.1103/PhysRevB.84.195133 PACS number(s): 73.21.La, 73.63.Kv, 68.37.Ef

I. INTRODUCTION

Semiconductor nanocrystals (NCs) have a highly efficient, tunable, and spectrally narrow luminescence that makes them attractive for various light-emitting based applications, such as biolabeling or LEDs.[1–4] However, until very recently, they suffered from an intermittent quenching of their photoluminescence, which was assumed to be caused by an extra charge, most likely trapped on the surface of the NC.[5,6] Similarly, measurements of the tunneling current recorded on top of single semiconductor NCs placed in a double barrier tunnel junction (DBTJ) also exhibited noise that was attributed to charge fluctuations in the NC environment.[7,8] In order to reduce the trapping of charge carriers on the NC surface, great efforts have therefore been focused on the growth of an inorganic shell around the NCs.[9–13] While continuous photoluminescence has been found when a shell protects the NC core,[14,15] the addition of the shell leads to the formation of heterostructures, where the localization of the charge carriers may be significantly modified with respect to the core only.[16–18] As good control over the optical properties of heterostructured NCs is required for their successful application, the knowledge of the carrier localization in heterostructured NCs necessitates in-depth studies of their electronic structures, which can be achieved with scanning tunneling spectroscopic experiments.[19–21]

A prototypical case concerns PbSe NCs that emit in the infrared energy range and suffer from a reduction of the quantum yield with time due to the oxidation of the NC surface.[22] Based on the reported enhancement of the brightness stability when the PbSe core is embedded in a CdSe shell,[23] we have investigated PbSe/CdSe core-shell NCs by means of scanning tunneling spectroscopy (STS) at low temperatures. Tunneling spectroscopy on these systems is based on resonant tunneling across a DBTJ.[19,20] So far most of the experiments have dealt with asymmetric junctions, where the tip-NC distance was larger than the NC-substrate distance, giving access to the quasiparticle band gap of the NCs and to the energy separation between the lowest quantized levels of the conduction and valence bands.[21,24] However, with the addition of a shell, the potential drop across the tunneling junctions can be strongly modified, making the interpretation of the spectra more delicate.[25] Here, we show that the potential drop across both potential barriers is rather symmetric when we study PbSe/CdSe core-shell NCs with an intended shell thickness of 0.4 nm. As a result, for the majority of the NCs we find that the peaks observed in the tunneling spectra at both negative and positive voltages are related to the same charge carriers, corresponding to a unipolar transport regime.

We report similar results for CdSe/CdS dot-in-rod NCs,[26] indicating that the addition of a thin shell is appropriate to investigate the shell-filling regime and to measure charging energies involving the lowest energy levels of the NCs. As the nature of the charge carriers contributing to the tunneling current varies from NC to NC, the shell structure of the PbSe/CdSe core-shell NCs has also been investigated by photoemission spectroscopy. It reveals the existence of a partial shell, which accounts for the fluctuations of the potential drop measured across the tunnel barriers, depending on the orientations that the NCs have adopted on the substrate.

II. THEORETICAL BACKGROUND

When a quantum dot is weakly coupled to two leads in a DBTJ, the potential distribution in such a system is usually characterized by the lever arm η. This quantity corresponds to the ratio between the potential drop across the NC-tip junction and the voltage applied to the gold surface with respect to the tip held at virtual ground. Based on the capacitance model shown in Fig. 1(a) where the core-shell NC exhibits the properties of a type-I heterostructure, the lever arm is given by the ratio between the capacitance C_1 and the sum of the

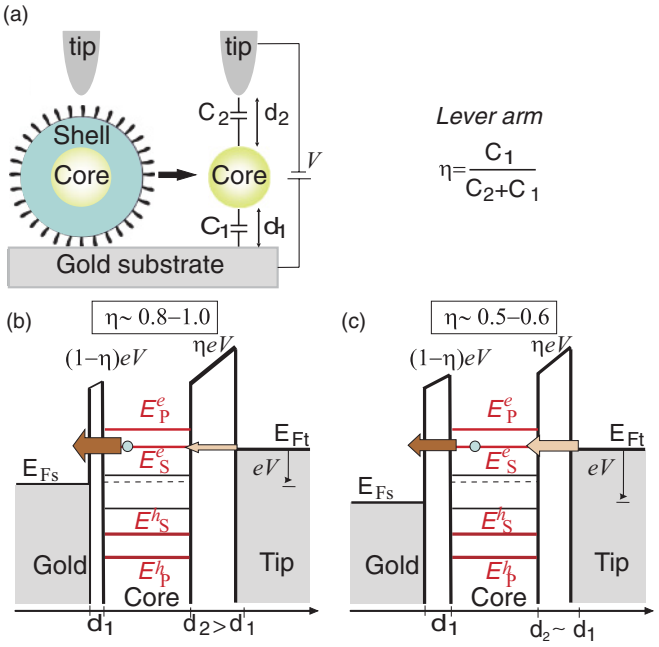

FIG. 1. (Color online) (a) Schematic and equivalent circuit of a double barrier tunnel junction, where a core-shell NC is inserted between a STM tip and a gold substrate. The lever arm, the applied voltage, the capacitance, and the thickness of both barriers are labeled η, V, C_1, C_2, d_1, and d_2, respectively. (b), (c) Energy-band diagrams of the system when η is high or low. The electron/hole S and P energy levels of the core, the Fermi levels of the tip E_{Ft}, substrate E_{Fs}, and NC (dashed segment) are indicated, as well as the magnitude of the transmission probability across both barriers (arrows with different widths).

capacitance C_1 and C_2: $\eta = C_1/(C_1 + C_2)$. When the tip is far from the NC, C_2 is usually much smaller than C_1 and the lever arm is close to 1. In this case the transmission probability across the second potential barrier is much smaller than the transmission probability across the first potential barrier [see Fig. 1(b)], and the measurements of peaks in the tunneling spectra correspond to single-electron energy levels. In such a regime, usually named the shell-tunneling regime, the lowest peaks observed on both sides of the apparent band gap, also called the zero-conductance region, are related to the electron and hole ground states, respectively.[21] Writing the energies of both levels relative to the Fermi energy as e_1 and h_1, respectively, these peaks occur at the voltages $V^+_{e_1}$ and $V^-_{h_1}$ given by

$$V^+_{e_1} = \frac{e_1 + \Sigma_e}{e\eta} \tag{1}$$

$$V^-_{h_1} = \frac{h_1 - \Sigma_h}{e\eta}. \tag{2}$$

Here, Σ_e and Σ_h stand for the polarization energy of the electron and the hole, respectively. It follows that in this case the lever arm can be deduced from the ratio between the quasiparticle band gap $E^{\mathrm{qp}}_{\mathrm{Gap}}$ ($=e_1 - h_1 + \Sigma_e + \Sigma_h$) and the measured zero-conductance region $e(V^+_{e_1} - V^-_{h_1})$:

$$\eta = \frac{E^{\mathrm{qp}}_{\mathrm{Gap}}}{e\left(V^+_{e_1} - V^-_{h_1}\right)}, \tag{3}$$

where the single-particle band gap $E_{\mathrm{Gap}} = e_1 - h_1$ and the polarization energies can be determined numerically.[27]

An alternative tunneling regime may occur when C_2 becomes comparable to C_1, which means that the lever arm approaches 0.5. In the simplified model of Fig. 1, this can arise when the thickness of both tunnel barriers are similar. Then, the transmission probability across the barriers becomes comparable [Fig. 1(c)], a situation favorable for charging the NC. Moreover, if the Fermi level in the NC is not positioned midgap, then the same state can contribute to the tunneling current on each side of the zero-conductance region, leading to unipolar transport.[27] In the case of tunneling through the electron level e_1, this results in a conductance peak at a negative bias $V^-_{e_1}$ given by

$$V^-_{e_1} = -\frac{e_1 + \Sigma_e}{e(1-\eta)}. \tag{4}$$

Alternatively, in the case of tunneling through hole level h_1, the conductance peak occurs at a positive bias $V^+_{h_1}$ given by

$$V^+_{h_1} = -\frac{h_1 - \Sigma_h}{e(1-\eta)}. \tag{5}$$

Combining Eqs. (1) and (4), one sees that for unipolar electron transport, the lever arm can be directly obtained from the tunneling spectrum as

$$\eta = \frac{V^-_{e_1}}{V^-_{e_1} - V^+_{e_1}}. \tag{6}$$

With unipolar hole transport, one finds a similar expression:

$$\eta = \frac{V^+_{h_1}}{V^+_{h_1} - V^-_{h_1}}. \tag{7}$$

A proper identification of the peaks at positive and negative bias as corresponding to electron or hole tunneling is possible by looking at the change in the peak voltage as a function of the lever arm. At positive bias, it is easily demonstrated that $V^+_{e_1}$ will increase while $V^+_{h_1}$ will go down if the lever arm is reduced. At negative bias, the opposite is true, i.e., $V^-_{h_1}$ will become more negative and $V^-_{e_1}$ less negative upon reducing η.

III. EXPERIMENTAL RESULTS

PbSe core particles were synthesized according to literature methods.[28] The formation of the shell was achieved through a cationic exchange of Pb by Cd, where a mixture of Cd oleate is added to the PbSe NC suspension in toluene heated at 100 °C.[29] High resolution transmission electron microscopy (HR-TEM) indicated that the reaction left unchanged the mean diameter of the NCs at 7.9 nm. The reaction was stopped when the replacement of the outermost Pb atoms by Cd cations resulted in a shell thickness of 0.4 nm, corresponding to a steady blue shift in the photoluminescence spectra due to the reduction of the core size. CdSe/CdS dot-in-rod NCs were also synthesized, as described in Refs. 26 and 30, and characterized by optical spectroscopy and HR-TEM. The CdSe core had a diameter of 3.5 nm, and the thickness of the CdS shell was estimated to be between 0.3 and 0.4 nm. The average length of the rod is 20.1 nm.

Langmuir-Blodgett (LB) monolayers were formed by dropping the resulting NCs, suspended in $CHCl_3$ on a Langmuir

trough, followed by a single-stroke compression of the Langmuir film.[31] Transfer to a flame-annealed Au(111) substrate was typically achieved at a surface pressure of 25 mN/m. The sample was finally loaded in an ultra high vacuum (UHV) system containing a low-temperature scanning tunneling microscope (LT STM, Omicron Nanotechnology). The spectroscopic tunneling experiments were performed on individual NCs by measuring the dynamic differential conductance using a lock-in amplifier ($V_{\text{mod p-p}} = 11$–15 mV, $f_{\text{mod}} = 0.5$–1.0 kHz) at a temperature of 4.8 K. Typically a large number of curves were acquired above a single NC under identical feedback conditions. In order to minimize the influence of the charge fluctuations on the level broadening, averaging was restricted to curves, where the main peaks are shifted by less than ± 4 mV between the curves.[32]

For the study of the core levels by x-ray photoelectron spectroscopy (XPS), we used a monochromatic Al Kα x-ray source and analyzer-pass energy of 11.75 eV. Under these conditions the overall resolution as measured from the full width at half maximum (FWHM) of the Ag 3d5/2 line was 0.55 eV. The binding energy scale was calibrated using the Au 4f7/2 line at 84.0 eV. The acceptance angle of the analyzer was set to 14°, and the angle between the incident x rays and the analyzer was 90°. The detection angle of the photoelectrons was 45°. The core-level decomposition was made with a minimum number of peaks, fitted with Voigt functions after standard Shirley background substraction. The spin-orbit splitting for the Cd 4*d*, Se 3*d*, and Pb 5*d* peaks was set at 0.67 ± 0.05 eV, 0.85 ± 0.05 eV, and 2.61 ± 0.05 eV, respectively.[33–36]

Figure 2 shows a constant current height image of a LB monolayer of PbSe/CdSe core-shell NCs transferred onto a Au(111) surface. The NCs have a two-dimensional close-packed arrangement with local hexagonal ordering, as seen in the inset of Fig. 2. From the Fourier transform of large scale STM images, such as the one of Fig. 2, an average center-to-center spacing of 8.1 ± 0.5 nm is found. This separation is slightly larger than the mean NC diameter of 7.9 nm, but it is smaller than the separation usually found between NCs that are deposited into an array by the drop casting method.[37] This suggests that the oleic acid ligands are more strongly compressed in the LB monolayer.

As the mean interdot separation is consistent with the mean NC diameter, we determine the size of the NCs directly from high resolution STM images. By positioning the tip above a PbSe/CdSe NC with a diameter of 9.8 nm, sweeping the tip-substrate voltage with the feedback loop open allows us to measure a differential conductance spectrum, as shown in Fig. 2(b). It reveals a zero-conductance gap surrounded by sequences of peaks at positive and negative sample voltages. These conductance peaks are caused by the tunneling of charge carriers through the quantized levels of the NC. Interestingly, the zero-conductance gap and the energy-level separation appear to be much larger than the ones measured for a slightly smaller PbSe NC for similar feedback loop settings.

Indeed, as the shell thickness is 0.4 nm, the core size of the PbSe/CdSe is bigger by 0.2 nm than the diameter of the PbSe NC. A reduction of the confinement effects should lead to a smaller apparent band gap for the PbSe/CdSe NC with respect to the PbSe NC. Instead, we observe an increase. This

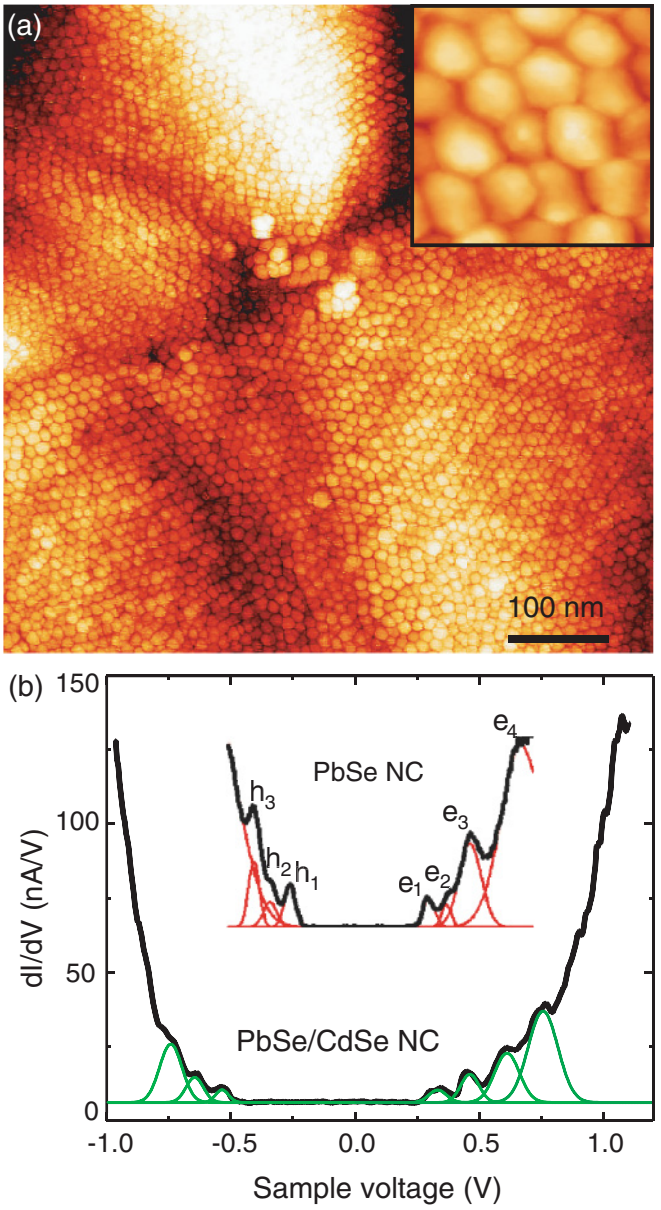

FIG. 2. (Color online) Large scale STM image of PbSe/CdSe NCs transferred onto a Au(111) surface by the Langmuir-Blodgett technique. Inset: High resolution STM image of the close-packed NC monolayer. The images were acquired at a sample voltage V_S of +2.0 V, a tunneling current I_{set} of 10 pA. (b) Tunneling spectra measured on a PbSe/CdSe NC with a diameter of 9.8 nm and a PbSe NC with a diameter of 8.7 nm. The spectra are fitted with Gaussian functions, and the resonances are labeled h_1 to h_3 for the valence levels and e_1 to e_4 for the conduction levels of the PbSe NC. Feedback conditions: PbSe NC, $V_S = +1.2$ V, $I_{\text{set}} = 0.5$ nA; PbSe/CdSe NC, $V_S = 0.7$ V, $I_{\text{set}} = 0.4$ nA.

behavior can result from a change of the potential distribution between both potential barriers. Without any shell the DBTJ is typically asymmetric, with the tip-NC distance much larger than the NC substrate, resulting in a lever arm close to 1. In contrast, with the addition of a shell around the core, the NC-substrate distance increases. The transmission probability across the DBTJ gets smaller, and working at similar tunneling current setpoints requires a decrease of the tip-NC distance. If

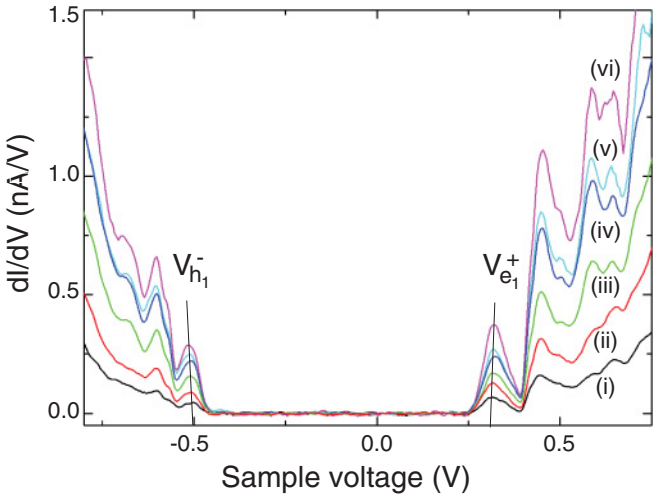

FIG. 3. (Color online) Set of differential conductance spectra measured on a PbSe/CdSe NC with a diameter of 8.5 nm. The feedback parameters were $V_S = +1.2$ V and $I_{set} = 0.5$ nA (i), 1.0 nA (ii), 1.5 nA (iii), 2.0 nA (iv), 2.5 nA (v), and 3.0 nA (vi). The peaks labeled $V_{h_1}^-$, $V_{e_1}^+$ correspond to the tunneling of holes and electrons through the hole and electron ground states, respectively. The oblique segments are used as guides to the eye to highlight the shift of the peak positions with increasing I_{set}.

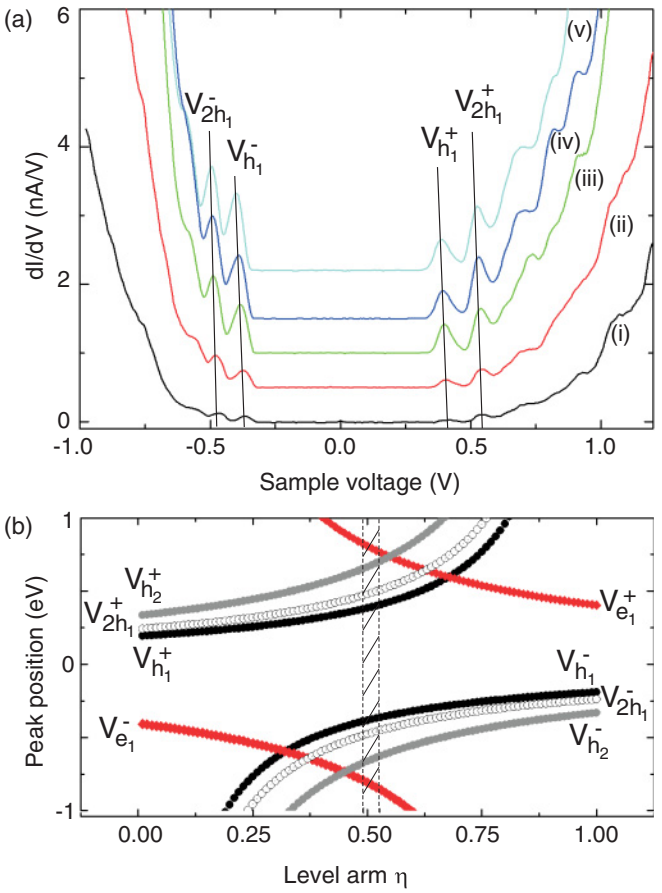

FIG. 4. (Color online) (a) Set of differential conductance spectra measured on a PbSe/CdSe NC with a diameter of 8.5 nm. The feedback parameters were $V_S = +1.2$ V and $I_{set} = 0.5$ nA (i), 1.0 nA (ii), 2.0 nA (iii), 2.5 nA (iv), and 3.0 nA (v). The peaks labeled $V_{h_1}^-$, $V_{2h_1}^-$, $V_{h_1}^+$, $V_{2h_1}^+$ correspond to tunneling through the hole ground state with zero and one hole at negative and positive bias. The oblique segments are used as guides to the eye to highlight the shift of the peak positions with increasing I_{set}. (b) Variation of the peak position as a function of the lever arm η. The hole first excited and electron ground states measured at negative and positive voltages are respectively labeled $V_{h_2}^-$, $V_{h_2}^+$, $V_{e_1}^-$, and $V_{e_1}^+$. The shaded region corresponds to the range of lever arms measured in (a).

we assume a homogeneous shell thickness, then the width of both potential barriers becomes comparable, and we should expect the lever arm to decrease and even approach 0.5. As described previously, when the Fermi level in the NC is midgap, a decrease of the η may cause an increase of the zero-conductance gap, since the apparent gap corresponds to the quasiparticle gap divided by the lever arm.

While a more symmetric potential distribution across the DBTJ significantly affects the width of the zero-conductance region, it generally complicates the assignment of the peaks.[27,38] Indeed, depending on the position of the Fermi level in the band gap, the same type of carriers can contribute to the tunneling current on both sides of the zero-conductance gap before the occurrence of a combined electron-hole transport. To determine whether the quantized levels at the edge of the zero-conductance region are related to the electron or hole ground state, a set of differential conductance spectra acquired with increasing setpoint currents can be measured. If the separation between the peaks surrounding the zero-conductance region increases with higher set-point currents, then the peaks arise from the contribution of the hole and electron ground states at negative and positive sample voltages, respectively.[27]

Such a result is clearly seen in Fig. 3, where the shift of the peaks $V_{h_1}^-$ and $V_{e_1}^+$, with increasing set-point currents, induces a slight widening of the apparent band gap. Measuring the diameter of the NC in the topographic image and assuming that the electronic properties of the core are not strongly affected by the shell, a band gap E_G of 0.550 eV and a polarization energy Σ of 23 meV were respectively calculated for a PbSe core size of 7.7 nm.[21,32] From the measurement of the zero-conductance region, the lever arm was found to decrease from 0.72 to 0.71 when the set-point current changed from 0.5 nA to 3.0 nA. In such a case, the potential predominantly drops across the tip-NC junction, i.e., the NC-substrate junction has the largest capacitance.

However, a large number of spectra recorded on other NCs did not show this behavior. Instead, some NCs exhibited a set of differential conductance spectra similar as the one shown in Fig. 4(a). While the overall peak structure of the spectra is the same whatever the set-point current is, the shift of the peaks on both sides of the zero-conductance region readily differs in comparison with Fig. 3. Indeed an increase of the set-point current causes a shift of the lowest peak measured at positive bias toward smaller sample voltages. This shift is opposite to the expected shift that should occur if electrons were tunneling through the conduction-band ground state for smaller and smaller lever arms.[27] We thus identify it as the contribution of the hole ground state h_1 to the tunneling current.

In order to confirm that the onsets of the differential conductance are caused by tunneling through the hole ground

state at negative and positive voltages, the evolution of the zero-conductance region can be analyzed as a function of the lever arm. From the position of $V_{h_1}^+$ and the separation of $V_{h_1}^+$ and $V_{h_1}^-$, we can deduce the lever arm, based on Eq. (7). For the lowest set-point current, we measure a lever arm of 0.53. Then, the lever arm monotonously decreases to 0.49 as the set-point current increases. Knowing the diameter of the NC from the topographic STM image and assuming that the very thin layer of CdSe does not significantly affect the core electronic structure, we calculate a quasiparticle gap of 596 meV for a PbSe core with a diameter of 7.7 nm, the band gap E_G, and the polarization energy Σ being 550 meV and 23 meV, respectively.[32] As a result, we find $h_1 - E_F = -169$ meV, with a variation of ± 1 meV for the range of set-point currents used in the experiments.

The theoretical knowledge of the band gap then yields $e_1 = 381$ meV. Although the peaks $V_{e_1}^+$ and $V_{e_1}^-$, that correspond to the tunneling of electrons from the conduction-band ground state at positive and negative voltages, respectively, are not provided by the spectroscopic experiments, they can be deduced from the energy of level e_1,

$$V_{e_1}^+ = \frac{(e_1 - E_F) + \Sigma}{\eta} \tag{8}$$

and

$$V_{e_1}^- = -\frac{(e_1 - E_F) + \Sigma}{1 - \eta}. \tag{9}$$

Based on Eqs. (2), (5), (8), and (9), the position of the peaks $V_{h_1}^-$, $V_{h_1}^+$, $V_{e_1}^+$, and $V_{e_1}^-$ can be plotted as a function of the lever arm, as shown in Fig. 4(b). In the shaded area of Fig. 4(b), which corresponds to the range of lever arms deduced from Fig. 4(a), $V_{e_1}^+$ and $V_{e_1}^-$ are clearly higher and lower than $V_{h_1}^+$ and $V_{h_1}^-$, respectively, demonstrating that only holes are allowed to tunnel on both sides of the zero-conductance region.

We also note that the second peak observed at positive and negative voltages shifts in the same way as the set-point current increases. This peak could arise from the contribution of the first hole excited state, labeled $V_{h_2}^-/V_{h_2}^+$ depending on the bias. However, a lever arm around 0.5 indicates that both C_1 and C_2 are of similar magnitude. Therefore, it is reasonable to think that the tip is quite close to the NC, the tunnel barriers being symmetric and mainly made up of the CdSe shell and the capping organic ligands. In such a configuration the probabilities to tunnel into or out of the NC are similar, implying that a hole can already reside in the NC when a new hole tunnels into the NC. The second peak could then be caused by the charging energy required to keep two holes on the ground state. It is labeled $V_{2h_1}^-$ and $V_{2h_1}^+$ depending on the bias sign. To discriminate between the first excited state and the charging of the hole ground state, we calculated the position of the first excited state and the charging energy as a function of η.[32] As shown in Fig. 4(b), the spectral separation between $V_{h_2}^-$ and $V_{h_1}^-$ for a lever arm around 0.5 is about 270 meV. Conversely, the spectral separation between $V_{2h_1}^-$ and $V_{h_1}^-$ is smaller, around 100 meV. This value is consistent with the separations found between the first and second peaks at negative voltages in Fig. 4(a). Therefore, we attribute the second peak at negative voltage to the tunneling of a second hole into the hole ground state that already bears one hole and find a charging energy of 50 meV, consistent with the theoretical value of 48 meV.

At positive voltage, the energy separation between the first and second peaks is slightly higher by about 20 meV, because this quantity is divided by $1 - \eta$ instead of η. Then, we identify the second peak $V_{2h_1}^+$ as a charging transition. Finally, the third peak observed at negative voltage, which mostly appears as a shoulder, is separated by the same amount of energy as $e(V_{2h_1}^- - V_{h_1}^-)$. We reasonably attribute it to the tunneling of a third hole into the hole ground state that already contains two holes, in agreement with an energy level that can accommodate up to eight holes due to its degeneracy.

The opposite regime where only electrons tunnel on both sides of the zero-conductance region can also be found, albeit in much smaller cases. Figure 5(a) shows an example of a set of spectroscopic measurements performed with increasing set-point currents where the onset peaks shift toward higher sample voltages. This behavior allows us to attribute the peaks $V_{e_1}^+$ and $V_{e_1}^-$ to the contribution of the electron ground state

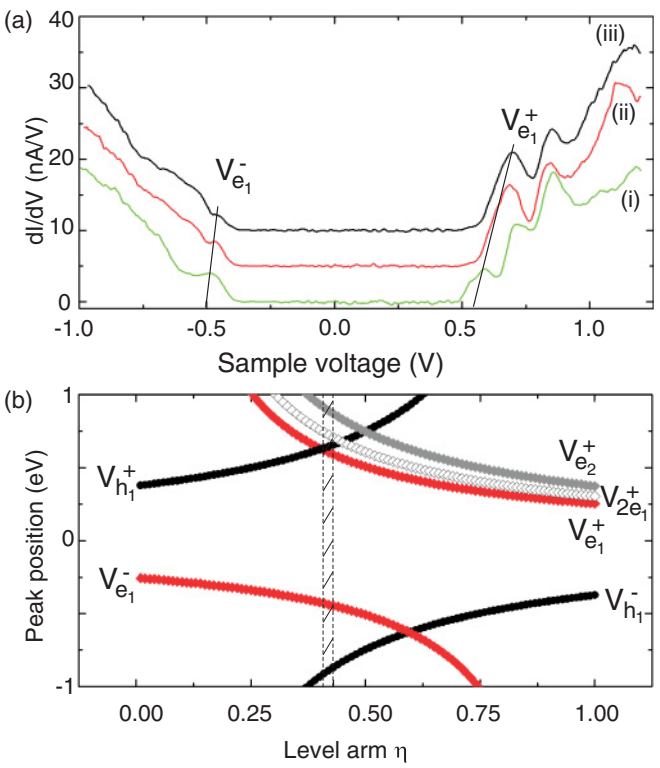

FIG. 5. (Color online) Set of differential conductance spectra measured on a PbSe/CdSe NC with a diameter of 8.1 nm. The feedback parameters were $V_S = +1.2$ V and $I_{set} = 1$ nA (i), 2.5 nA (ii), and 2.8 nA (iii). The peaks labeled $V_{e_1}^-$, $V_{e_1}^+$ correspond to the tunneling of electron from the electron ground state at negative and positive bias. The oblique segments are used as guides to the eye to highlight the shift of the peak position with increasing I_{set}. (b) Variation of the peak position as a function of the lever arm η. The peaks labeled $V_{h_1}^-$, $V_{h_1}^+$, $V_{2e_1}^+$, and V_{e2}^+ correspond to tunneling through the hole ground state at negative and positive bias, the electron ground state that holds one electron, and the electron first excited at positive bias. The shaded region corresponds to the range of lever arms measured in (a).

at positive and negative voltages. In order to determine the origin of the second peak observed at positive voltage, we can deduce the lever arm using Eq. (6). At low set-point current, we measure a lever arm of 0.43. Then, the lever arm decreases to 0.40 as the set-point current increases.

Based on the diameter of the NC, 8.1 nm, which corresponds to a core size of 7.4 nm, the charging energy should be 50 meV. Translating the charging energy into voltage yields a voltage separation between the first and second peaks of 116 meV, as shown in Fig. 5(b). Such a separation, which is smaller than the first electron intraband transition of 120 meV divided by η, is close to the energy separation of 129 meV found at low set-point current. Therefore we identify the second peak to the transfer of an electron into the electron ground state that already hosts one electron. Similarly the energy separation between the second and third peak is 136 meV, suggesting that the second peak is related to the charging of the electron ground state, which already holds two electrons. Interestingly, at a lever arm just smaller than 0.4, a hole and an electron are likely to be transferred to the NC quantum levels simultaneously. As there are some uncertainties on the NC size and thus on the peak positions, such a situation might explain why the third peak disappears when the set-point current increases in Fig. 5(a).

IV. DISCUSSION

In contrast to most tunneling spectroscopic measurements performed on PbSe quantum dots,[21,32] the addition of a very thin shell of CdSe leads to the accumulation of charge carriers in the NC, due to similar transmission probabilities across both tunnel barriers. While the lever arm is close to 0.5 for more than 80% of the NCs that were probed, the Fermi level is not positioned at the same energy in the band gap of the NC. It might be closer to the valence-band edge [see, for example, Fig. 4(a)] or lie in the upper part of the band gap [example of Fig. 5(a)]. In addition the latter example reveals that the lever arm can be lower than 0.5, indicating that the potential drop predominantly occurs between the NC and the substrate. Such a result suggests that the tip-NC distance becomes smaller than the NC-substrate distance. Therefore the shell thickness would not be uniform all around the PbSe core.

In order to clarify this point, x-ray photoemission spectroscopic experiments have been performed on the same sample. For comparison, two additional types of NCs were investigated: a sample consisting of PbSe NCs only and a sample with PbSe/CdSe core-shell NCs, where the thickness of the shell was 2 nm. Both samples were not annealed prior to the XPS experiments to avoid any phase transformation of the NCs.[39] When the XPS spectra of all three samples are compared (Fig. 6), the successful cation exchange between Pb and Cd, at the surface of the NCs considered in the STS study, is demonstrated through (i) the presence of Cd 4*d* photoelectron lines for both types of NCs containing Cd, and (ii) the occurrence of a Se 3*d* peak that shows an intermediate lineshape between the lineshape obtained for the PbSe NCs and the PbSe NCs surrounded by a thick CdSe shell. Indeed, as Se atoms are bound to both Pb and Cd atoms, two spin-orbit split doublets are required in order to decompose the Se 3*d* core level (binding energies of 53.82 and 54.21 eV for the two first peaks). Moreover, the fitting procedure shows that the lineshape of the PbSe/CdSe NCs with a thin shell is closer to the lineshape of the Se 3*d* peak for PbSe NCs, suggesting that the NCs contain a higher quantity of Se atoms bound to Pb atoms than Se atoms bound to Cd atoms. Such a result is consistent with a thin layer of CdSe.

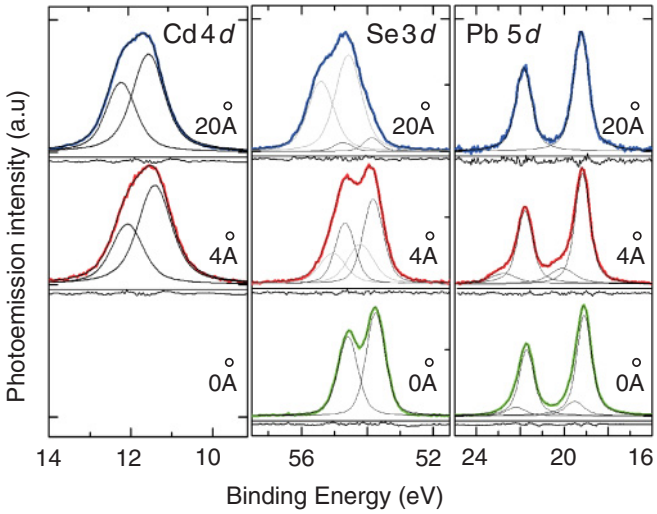

FIG. 6. (Color online) Background-substracted Cd 4*d*, Se 3*d*, and Pb 5*d* core-level spectra and fits of PbSe/CdSe NCs with different CdSe shell thickness given in angström, as indicated in the graph. The residual plots are also shown below each core-level spectrum.

As for the Pb 5*d* core level, the Pb $5d_{5/2}$ (lower binding energy) and Pb $5d_{3/2}$ (higher binding energy) peaks are decomposed with a single component that is related to the Pb atoms bound to Se atoms in the core for the NCs with the thick shell. For the Pb $5d_{5/2}$ peak, this component is centered at a binding energy of 19.27 eV and has a FWHM of 0.84 eV. Conversely, the Pb $5d_{5/2}$ peak of the PbSe NCs requires the use of two components. From the comparison of the peak position with the one obtained for the PbSe/CdSe NCs with a thick shell, we attribute the component at the lowest binding energy, centered at 19.10 eV (FWHM 0.80 eV), to the bulk contribution of the NCs. The second peak with the highest binding energy, centered at 19.53 eV (FWHM 1.05 eV), is thus related to the surface. Its position as well as its width would correspond to surface Pb atoms bound to oxygen, in agreement with results reported for the oxidation of PbSe.[40] Such PbO species exist due to the passivation of the NC surface with ligands and also because the surface of the NCs might oxidize during the transfer of the NCs in air.

Looking at the Pb peaks of the NCs considered in the STS experiments, a single spin-orbit split doublet does not allow us to satisfactorily decompose the Pb 5*d* core level. In addition to the Pb $5d_{5/2}$ component centered at 19.16 eV, a broad shoulder exists at a higher binding energy of 20.10 eV. While we attribute this shoulder to PbO species, a shift of this component with respect to the component found for the nonannealed PbSe NCs indicates that the degree of oxidation of the Pb atoms is different. The surface Pb atoms of the PbSe/CdSe NCs with a thin CdSe shell would be more oxidized. Such a result can

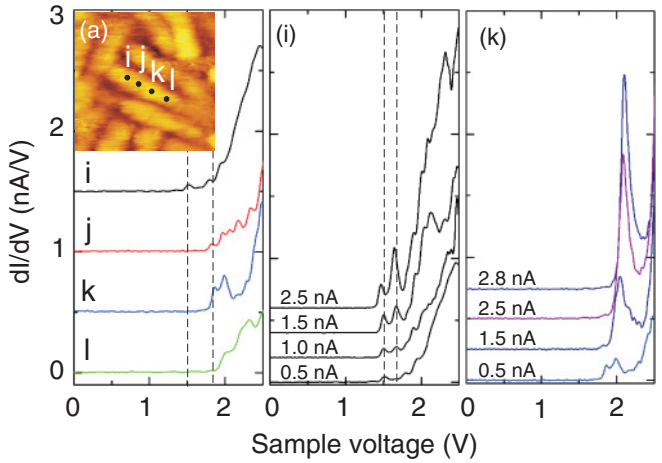

FIG. 7. (Color online) (a) Set of tunneling spectra measured along a CdSe/CdS dot-in-rod NC with a set-point current of 0.5 nA. Inset: STM image of the close-packed NC monolayer. (i) and (k) Set of differential conductance spectra acquired at positions (i) and (k) along the NC for increasing set-point currents from 0.5 to 2.8 nA. The vertical dashed lines are used as guides to the eye to highlight the peak separation or shifts in peak position.

be understood as follows: the annealing of the NCs in UHV, before the STM experiments, leads to the partial desorbtion of ligands. Then, the transfer in air between the LT STM and the XPS system causes a stronger oxidation of the Pb atoms on the NC surface due to the absence of ligands.

As the exchange of Pb by Cd was very limited in time to obtain an equivalent shell thickness smaller than one monolayer for these NCs (the lattice parameter of zincblende CdSe being 6.05 Å), the observation of this shoulder means that a part of the NC surface exposed uncovered PbSe facets, where the Pb atoms are bound to O species. Such results indicate that a large number of NCs have a partial CdSe shell, leaving one or several PbSe facets unprotected, in agreement with TEM images of similar NCs where the shell was even thicker.[29] Such fluctuation in the shell thickness from one NC to another one might explain why three types of tunneling spectra have been found. It also accounts for the variations of the Fermi-level position, as the pinning of this level certainly changes with the structural and chemical composition of the NC surface. Depending on the location of the unprotected PbSe facets in the DBTJ, either exposed to the STM tip or below the NC, against the substrate, the lever arm can greatly vary. In some particular cases, it can become smaller than 0.5, in contrast to the range of lever arms that are usually measured on semiconductor NCs using STS.[21,32]

Finally, we think that the results obtained for the PbSe/CdSe core-shell NCs are quite general for tunneling spectroscopic measurements performed on core-shell nanostructures. As an additional example, we have investigated CdSe/CdS dot-in-rod NCs by means of tunneling spectroscopy. Figure 7 shows spatially resolved conductance spectra acquired at four different positions along a nanorod. Focusing on the onset of the curves at positive bias, we measure a shift of 0.39 eV between the lowest peak observed in region (i) and the onset of the first step in region (l). While such a result suggests that the core is located in region (i), discriminating between the contribution of electron or hole states to the conductance spectrum requires us to study the change of the onsets as a function of the set-point current.

As seen in Fig. 7(i), an increase of the set-point current leads to a shift of the lowest peak toward smaller and smaller voltages. This shift is opposite to the expected shift that should occur if electrons were tunneling through the conduction-band ground state of the CdSe core for decreasing lever arms, as already explained in the case of the PbSe/CdSe core-shell NCs. We thus identify the lowest peak in spectrum (i) as the contribution of the hole ground state to the tunneling current. Conversely, in the middle of the nanorod, the onset of the spectra (k) shifts toward higher energies as the set-point current increases, indicating that away from region (i) the current is related to electron states at positive sample voltage.

The bulk band gap of CdSe is 1.84 eV at 5 K and should reside inside the larger CdS band gap (2.58 eV at 5 K). Numerous experimental results have shown that the CdSe/CdS interface is characterized by a large valence-band offset, which confines the hole wave function to the core region of the nanorod.[41–43] Assuming a NC Fermi level in the vicinity of the valence-band edge for the CdSe core, we expect, for a lever arm close to 0.5, the contribution of the hole ground state at positive sample voltages before the tip Fermi level becomes aligned with the lowest electron state. It should be different when the tip is above the CdS rod. Indeed, due to the large valence-band offset between CdSe and CdS, the CdS valence-band edge is positioned much below the NC Fermi level. Then the tip-Fermi level is more likely to be first resonant with the electron ground state at positive bias, as seen in Fig. 7(k).

Remarkably, the second peak observed in Fig. 7(i) also shifts in the same direction as the first peak. It is again related to the contribution of a hole state. While the observation of a doublet is reminiscent of the two-fold degenerate electron *S* level in CdSe NCs, any ambiguities in the assignment of the peaks can thus be cleared up by performing tunneling spectroscopic measurements with different set-point currents.

V. CONCLUSION

In conclusion we have investigated the electronic structure of PbSe/CdSe core-shell NCs and CdSe/CdS dot-in-rod NCs by means of STS. For a large amount of NCs, we have found a unipolar transport regime, where only one type of charge carriers contribute to the tunneling current on each side of the zero-conductance gap. In this case the width of the zero-conductance region is not related to the quasiparticle band gap of the NCs. Instead, the determination of the peak position on both sides of the zero-conductance region provides a straightforward measurement of the lever arm. Lever-arm values around 0.5 have usually been obtained, indicating similar capacitances for both tunnel junctions. Such configuration, where the tip-NC and NC-substrate distances are similar and both tunnel junctions consist of the same dielectric materials, suggests that the probability for a carrier to tunnel into or out of the NC is almost the same, favoring the charging of the NCs. A charging energy on the order of 50 meV was measured for PbSe/CdSe core-shell NCs with

a mean core diameter around 7.5 nm, consistent with the charging energy expected for PbSe NCs with similar sizes. Therefore, the addition of a very thin shell around the core of semiconductor NCs offers the possibility to study transport regimes that are hardly accessible without the shell.

ACKNOWLEDGMENTS

This work was supported by the European Community ("HERODOT" project, Grant No. PITN-GA-2008-214954) and Nord Pas de Calais region. Z.H. acknowledges the Belgian Science Policy (IAP 6.10 photonics@be).

*bruno.grandidier@isen.iemn.univ-lille1.fr

[1] M. Bruchez Jr., M. Moronne, P. Gin, S. Weiss, and A. P. Alivisatos, Science **281**, 5385 (1998).
[2] R. C. Somers, M. G. Bawendi, and D. G. Nocera, Chem. Soc. Rev. **36**, 579 (2007).
[3] G. Konstantatos and E. H. Sargent, Nature Nanotechnol. **5**, 391 (2010).
[4] T.-H. Kim, K.-S. Cho, E. K. Lee, S. J. Lee, J. Chae, J. W. Kim, D. H. Kim, J.-Y. Kwon, G. Amaratunga, S. Y. Lee, B. L. Choi, Y. Kuk, J. M. Kim, and K. Kim, Nature Photonics **5**, 176 (2011).
[5] M. Nirmal, B. O. Dabbousi, M. G. Bawendi, J. J. Macklin, J. K. Trautman, T. D. Harris, and L. E. Brus, Nature **383**, 802 (1996).
[6] X. Brokmann, J.-P. Hermier, G. Messin, P. Desbiolles, J.-P. Bouchaud, and M. Dahan, Phys. Rev. Lett. **90**, 120601 (2003).
[7] L. Jdira, K. Overgaag, R. Stiufiuc, B. Grandidier, C. Delerue, S. Speller, and D. Vanmaekelbergh, Phys. Rev. B **77**, 205308 (2008).
[8] M. R. Hummon, A. J. Stollenwerk, V. Narayanamurti, P. O. Anikeeva, M. J. Panzer, V. Wood, and V. Bulovic, Phys. Rev. B **81**, 115439 (2010).
[9] B. Mahler, P. Spinicelli, S. Buil, X. Quelin, J.-P. Hermier, and B. Dubertret, Nat. Mater. **7**, 659 (2008).
[10] Y. Chen, J. Vela, H. Htoon, J. L. Casson, D. J. Werder, D. A. Bussian, V. I. Klimov, and J. A. Hollingsworth, J. Am. Chem. Soc. **130**, 5026 (2008).
[11] R. Osovsky, D. Cheskis, V. Kloper, A. Sashchiuk, M. Kroner, and E. Lifshitz, Phys. Phys. Lett. **102**, 197401 (2009).
[12] P. Spinicelli, S. Buil, X. Quélin, B. Mahler, B. Dubertret, and J.-P. Hermier, Phys. Rev. Lett. **102**, 136801 (2009).
[13] T. D. Krauss and J. J. Peterson, J. Phys. Chem. Lett. **1**, 1377 (2010).
[14] F. García-Santamaría, Y. Chen, J. Vela, R. D. Schaller, J. A. Hollingsworth, and V. I. Klimov, Nano Lett. **9**, 3482 (2009).
[15] X. Wang, X. Ren, K. Kahen, M. A. Hahn, M. Rajeswaran, S. Maccagnano-Zacher, J. Silcox, G. E. Cragg, A. L. Efros, and T. Krauss, Nature **459**, 686 (2009).
[16] J. Müller, J. M. Lupton, P. G. Lagoudakis, F. Schindler, R. Koeppe, A. L. Rogach, J. Feldmann, D. V. Talapin, and H. Weller, Nano Lett. **5**, 2044 (2005).
[17] M. G. Lupo, F. Della Sala, L. Carbone, M. Zavelani-Rossi, A. Fiore, L. Ler, D. Polli, R. Cingolani, L. Manna, and G. Lanzan, Nano Lett. **8**, 45828 (2008).
[18] P. Reiss, M. Protière, and L. Li, Small **5**, 154 (2009).
[19] U. Banin, Y. W. Cao, D. Katz, and O. Millo, Nature **400**, 542 (1999).
[20] L. Jdira, P. Liljeroth, E. Stoffels, D. Vanmaekelbergh, and S. Speller, Phys. Rev. B **73**, 115305 (2006).
[21] P. Liljeroth, P. A. Zeijlmans van Emmichoven, S. G. Hickey, H. Weller, B. Grandidier, G. Allan, and D. Vanmaekelbergh, Phys. Phys. Lett. **95**, 086801 (2005).
[22] J. W. Stouwdam, J. Shan, F. C. J. M. Van Veggel, A. G. Pattantyus-Abrham, J. F. Young, and M. Raydsepp, J. Phys. Chem. **111**, 1086 (2007).
[23] J. M. Pietryga, D. J. Werder, D. J. Williams, J. L. Casson, R. D. Schaller, V. I. Klimov, and J. A. Hollongsworth, J. Am. Chem. Soc. **130**, 4879 (2008).
[24] G. A. Grinbom, M. Saraf, C. Saguy, A. C. Bartnik, F. Wise, and E. Lifshitz, Phys. Rev. B **81**, 245301 (2010).
[25] I. Swart, Z. Sun, D. Vanmaekelbergh, and P. Liljeroth, Nano Lett. **10**, 1931 (2010).
[26] L. Carbone, C. Nobile, M. De Giorgi, F. D. Sala, G. Morello, P. Pompa, M. Hytch, E. Snoeck, A. Fiore, I. R. Franchini, M. Nadasan, A. F. Silvestre, L. Chiodo, S. Kudera, R. Cingolani, R. Krahne, and L. Manna, Nano Lett. **7**, 2942 (2007).
[27] Y. M. Niquet, C. Delerue, G. Allan, and M. Lannoo, Phys. Rev. B **65**, 165334 (2002).
[28] I. Moreels, K. Lambert, D. De Muynck, F. Vanhaecke, D. Poelman, G. Allan, and Z. Hens, Chem. Mater. **19**, 6101 (2007).
[29] K. Lambert, B. De Geyter, I. Moreels, and Z. Hens, Chem. Mater. **21**, 778 (2009).
[30] G. Rainò, T. Stöferle, I. Moreels, R. Gomes, J. S. Kamal, Z. Hens, and R. F. Mahrt, ACS Nano **5**, 4031 (2011).
[31] Y. Justo, I. Moreels, K. Lambert, and Z. Hens, Nanotechnol. **21**, 295606 (2010).
[32] K. Overgaag, D. Vanmaekelbergh, P. Liljeroth, G. Mahieu, B. Grandidier, C. Delerue, and G. Allan, J. Chem. Phys. **131**, 224510 (2009).
[33] A. Wall, Y. Gao, A. Raisanen, A. Franciosi, and J. R. Chelikowsky, Phys. Rev. B **43**, 4988 (1991).
[34] A. Lobo, T. Möller, N. Nagel, H. Borchert, S. G. Hickey, and H. Weller, J. Chem. Phys. B **109**, 17422 (2005).
[35] M. Cardona, D. W. Langer, N. J. Shevchik, and J. Tejeda, Phys. Phys. B **7**, 5228 (1973).
[36] F. R. McFreely, S. Kowalczyk, L. Ley, R. A. Pollak, and D. A. Shirley, Phys. Status Solidi B **58**, 127 (1973).
[37] P. Liljeroth, K. Overgaag, A. Urbieta, B. Grandidier, S. G. Hickey, and D. Vanmaekelbergh, Phys. Phys. Lett. **97**, 096803 (2006).
[38] B. Li, C. Zeng, J. Zhao, J. Yang, J. G. Hou, and Q. Zhu, J. Chem. Phys. **124**, 064709 (2006).
[39] D. Grodzińska, F. Pietra, M. A. van Huis, D. Vanmaekelbergh, and C. de Mello Donegá, J. Mat. Chem. **21**, 11556 (2011).
[40] A. L. Hagström and A. Fahlman, Phys. Scr. **16**, 432 (1977).
[41] J. Muller, J. M. Lupton, P. G. Lagoudakis, F. Schindler, R. Koeppe, A. L. Rogach, J. Feldmann, D. V. Talapin, and H. Weller, Nano Lett. **5**, 2044 (2005).
[42] A. Pandev and P. Guyot-Sionnest, J. Chem. Phys. **127**, 104710 (2007).
[43] N. J. Borys, M. J. Walter, J. Huang, D. V. Talapin, and J. M. Lupton, Science **330**, 1371 (2010).